Article

Not peer-reviewed version

Simultaneous Multiparameter Detection with Organic Electrochemical Transistors-Based Biosensors

Marjorie Montero-Jiménez , Jael R. Neyra Recky , Omar Azzaroni , Juliana Scotto * , Waldemar A. Marmisollé *

Posted Date: 5 December 2025

doi: 10.20944/preprints202512.0526.v1

Keywords: organic electrochemical transistors (OECTs); gate-potential cycling; multiparametric analysis; bioelectronic sensors; PEDOT

 doi:10.20944/preprints202512.0526.v1

Article

Simultaneous Multiparameter Detection with Organic Electrochemical Transistors-Based Biosensors

Marjorie Montero-Jimenez, Jael R. Neyra Recky, Omar Azzaroni, Juliana Scotto * and Waldemar A. Marmisollé *

Instituto de Investigaciones Fisicoquímicas Teóricas y Aplicadas (INIFTA), CONICET, Departamento de Química, Facultad de Ciencias Exactas, Universidad Nacional de La Plata, La Plata B1904DPI, Argentina

* Correspondence: jscotto@inifta.unlp.edu.ar (J.S.); wmarmi@inifta.unlp.edu.ar (W.A.M.)

Abstract

We present a methodology that enhances the analytical performance of organic electrochemical transistors (OECTs) by continuously cycling the devices through gate-potential sweeps during sensing experiments. This continuous cycling method (CCM) enables real-time acquisition of full transfer curves, allowing simultaneous monitoring of multiple characteristic parameters. We show that the simultaneous temporal evolution of several OECT response parameters (V_{TH}, $V_{G,gmax}$, and g_{max}) provides highly sensitive descriptors for detecting pH changes and macromolecule adsorption on OECTs based on PANI and PEDOT channels. Moreover, the method allows reconstruction of I_{DS}–time profiles at any selected gate potential, enabling the identification of optimal V_G values for maximizing sensitivity. This represents a substantial improvement over traditional measurements at fixed V_G, which may suffer from reduced sensitivity and parasitic reactions associated with gate polarization. Moreover, the expanded set of parameters obtained with the CCM provides deeper insight into the physicochemical processes occurring at both gate and channel electrodes. We demonstrate its applicability to monitoring polyelectrolyte and enzyme adsorption as well as detecting urea and glucose through enzyme-mediated reactions. Owing to its versatility and the richness of the information it provides, the CCM constitutes a significant advance for the development and optimization of OECT-based sensing platforms.

Keywords: organic electrochemical transistors (OECTs); gate-potential cycling; multiparametric analysis; bioelectronic sensors; PEDOT

1. Introduction

Among the wide range of analytical techniques currently available for the detection and quantification of substances in different types of samples, electrochemical sensors offer several advantages [1,2]. These include rapid, real-time responses, straightforward miniaturization, simple digitalization, ease of fabrication and scalability, and low cost, among others [3–7]. However, in many cases, the signals obtained from traditional electrochemical transduction methods (potentiometry, amperometric measurements, potential scanning techniques, etc.) are not sufficiently sensitive. As a result, strategies that amplify the signals are required in order to develop sensors capable of detecting analytes at low concentrations or in complex samples that must be diluted to minimize interfering species or appreciable matrix effects [8,9]. One of the most extensively developed approaches in recent years to increase the sensitivity of electrochemical sensors is based on field-effect transistors.

Basically, these transistors consist of a channel made of a conducting or semiconducting material connected to two terminals (source, S, and drain, D), together with a third electrode (gate, G) that is used to generate an electric field over the conducting channel (or to modulate its intensity) [8,10]. In this way, changes in the conductivity of the channel in the presence of the target analytes constitute

 doi:10.20944/preprints202512.0526.v1

the fundamental response underlying the transduction phenomenon. This response is typically more sensitive than in other technologies due to the possibility of modulation through the gate [9,11,12].

The specific mechanisms of signal transduction can vary widely and depend on the design and type of FET [13]. In particular, a widely used class for analytical purposes in solution is the electrolyte-gated (EG) FETs [14], in which both the gate and the channel are immersed in the same electrolyte—namely, the solution of interest [15]. Even within this class of EG-FETs, there are variants depending on the nature of the conducting channel. Thus, the channel may be graphene or reduced graphene oxide (g-FETs) [16,17], a monolayer or thin layer of organic molecules (o-FETs) [18,19], or a film of an electroactive polymer (organic electrochemical transistors, OECTs) [20–27]. In this latter case, changes in the gate potential lead to modifications in the redox state of the films, thereby altering their conductivity [8,28–32]. These redox changes are also accompanied by variations in the concentration of ions within the film [33]. For this reason, such materials are referred to as mixed ionic–electronic conductors [33–35]. Moreover, when the gate potential is dynamically modulated at a given scan rate, the transistor response depends on the coupling between the motion of charge carriers (holes and electrons) within the polymer and the movement of ions between the polymer film and the solution [8,28,36].

In the case of OECTs, a wide range of physicochemical phenomena can be exploited for sensing purposes [10,37,38]. On one hand, a substantial subset of studies relies on changes in the effective gate potential in the presence of a target analyte [39]. The analyte may directly modify the potential of the gate electrode if it is a redox-active species, such as H_2O_2 [40,41]; alternatively, it may induce a local pH change that produces an electrostatic effect on the gate potential, or even the specific binding of an ionic, molecular, or macromolecular species may alter the surface electric potential or the capacitance of the gate–solution interface [20,42–44]. On the other hand, transduction phenomena may also arise from the responsiveness of the channel to the analyte [45]. For instance, the presence of certain ions or molecules [46], or the interaction with macromolecules[47], can modify the redox state of the film, its charge state, or the impedance of the channel–solution interface, thereby producing changes that can be read through the OECT response [48,49].

All these phenomena can ultimately be detected as variations in the conductivity of the film under gate modulation [50,51]. Typically, such variations manifest as modifications of the transfer curves, i.e., the curves in which the drain–source current (I_{DS}) is recorded at a constant drain–source potential (V_{DS}) as a function of the gate potential (V_G) [52,53]. These I_{DS}–V_G curves are generally sigmoidal and can be characterized by several parameters, such as the maximum current (in the ON state), the maximum transconductance, g_{max}, and the threshold potential (V_{TH}). Of particular importance is the rate of change of conductivity with the gate potential, which is often quantified by the transconductance (gm), whose maximum value occurs at the inflection point of the I_{DS}–V_G curve (g_{max}).

Regardless of the specific transduction mechanism operating in a given sensor, the analytical response of the transistor is typically defined in terms of the changes observed as a function of the analyte concentration [50,52,54–57]. However, this response may be defined in multiple ways. One of the most common approaches is to monitor I_{DS} at a constant gate potential—often chosen near the maximum-transconductance point [58,59]. In this case, the current is recorded as a function of time or analyte concentration [40,43,60–62]. Nonetheless, because changes generally occur across the entire I_{DS}–V_G curve, they can also be monitored through variations in several characteristic parameters [63,64].

In this context, we present a method based on the continuous acquisition of I_{DS}–V_G curves, which allows the temporal evolution of all characteristic parameters to be extracted and even enables the reconstruction of chronoamperometric curves (I_{DS} vs. t) at any selected gate potential. This makes it possible to perform a simultaneous analysis of all parameters related to sensing events, whether they arise from ion intercalation, the interaction of macromolecules or proteins with the conducting channel, or the functional response of biosensors based on enzymatic activity in the presence of a target analyte.

 doi:10.20944/preprints202512.0526.v1

As we demonstrate here, this method allows post hoc selection of the parameters that best capture each process, enabling increased sensitivity through higher-amplitude responses or complementary analyses based on the simultaneous evolution of parameters that reflect different physicochemical aspects of the system.

2. Materials and Methods

2.1. Reagents

Polyallylamine hydrochloride (PAH, Mw ≈ 58kDa), 3,4 ethylenedioxythiophene (EDOT), aniline (ANI), poly (sodium 4-styrene sulfonate) (PSS) (Mw 70 kDa) and urea (99%) were acquired from Sigma Aldrich. Pyridine (99%) was obtained from Biopack. Iron (III) p-toluenesulfonate (38-42% in n-butanol) was purchased from Heraeus. Glucose oxidase (GOx, from aspergillus Niger) and Urease (from Canavalia ensiformis, Jack Bean, 200 KU) were obtained from Calzyme. Potassium chloride (KCl), n-butanol (99.4%), glucose, potassium hydroxide (KOH), sulfuric acid (H_2SO_4) and hydrochloric acid (HCl) were purchased from Anedra.

2.2. OECTs Preparation

The polymeric films were prepared on interdigitated electrodes (IDEs) (Microux ED-IDE1-Au, 10/10 μm electrode/gap). PEDOT-PAH films were synthesized by chemical polymerization as described in previous reports [65–67]. In summary, 5 μL of EDOT was mixed with 381 μL of an oxidant solution (220 μL of butanol, 16.5 μL of pyridine and 715 μL of Fe (III) p-toluenesulfonate), 1862 μL of butanol and 80 μL of a PAH solution (200 μL of ultrapure H_2O, containing 75 mg for polyelectrolytes analysis and 40 mg for the remaining measurements) [68]. The mixture was deposited onto IDEs using a spin coater (1 min of spin time, 1000 rpm of rotation rate and 500 rpm s^{-1} of acceleration) and the polymerization was carried out at 70 °C. Finally, the OECTs were washed with distilled water and dried with air.

PANI-based OECTs were prepared by electrochemical synthesis directly on the interdigitated electrodes. To this end, a 0.5 M aniline (previously distilled) in H_2SO_4 1 M solution was introduced into a conventional three-electrode cell, using the IDE as working electrode, a Pt wire as counter electrode and a commercial Ag/AgCl electrode as reference. Aniline polymerization was achieved by cycling the potential between -0.200 mV and 750 mV at 50 mV s^{-1}. The film was grown until it was thick enough to connect the drain and source terminals of the interdigitated electrodes (around 15 cycles were required).

2.3. Adsorption on Polymeric Films

The studied macromolecules, PSS and enzymes (urease and GOx), were electrostatically adsorbed on the polymeric film under flow conditions. First, the electrolyte (KCl) was injected, followed by the macromolecule of interest and finally the transistor was rinsed with KCl solution. All the solutions were injected with a flow rate of 30 μL min^{-1} for approximately 30 min for enzymes and 40 min for PSS.

2.4. SPR

Surface plasmon resonance (SPR) was performed using a SPR Navi 210 A (BioNavis Ltd, Tampere, Finland) and SPR gold (Au) substrates. PEDOT-PAH polymeric film was synthesized on SPR substrates by following the protocol used to modify the IDEs. The recording of angular scans with a laser of 785 nm was performed during the injection at a flow rate of 15 μL min^{-1} of the following solutions: 0.1 M KCl, then, 0.1 mg mL^{-1} PSS in 0.1 M KCl and the substrate rinsing with KCl. For enzyme adsorption, solutions of 10 mM KCl, next 1 mg mL^{-1} of enzyme in 10 mM KCl and finally 10 mM KCl were injected.

 doi:10.20944/preprints202512.0526.v1

2.5. Electrochemical Measurements

The electrochemical measurements were performed with a TEQ bipotentiostat. Static and flow experiments were performed in a Micrux Technologies cell. The static assays were performed with an Ag/AgCl in KCl 3M reference electrode as external gate while the flow experiments were carried out with an Ag/AgCl wire.

For transfer curves, the drain-source current (I_{DS}) was registered while the gate potential (V_G) was cyclically swept between the oxidized and the reduced state at a scan rate of 10 mV s^{-1}, under a constant drain-source potential (V_{DS}) of -50 mV.

2.6. Data Curation

In order to simplify and systematize the determination of the OECT characteristic parameters, Python programming was employed to perform data analysis. In particular, numpy, scipy and pandas libraries were used to process and organize data.

3. Results and Discussion

3.1. OECT Characteristic Parameters Determination

The determination of the OECTs characteristic parameters will be illustrated from the transfer curves obtained with a PANI channel that was cycled continuously sweeping the gate potential (V_G) at a low scan rate (v = 10 mV s^{-1}) in 1M HCl. A constant potential difference (V_{DS} = -50 mV) was applied between drain and source terminals while the I_{DS} was recorded (Figure 1A). With this procedure, we obtained the transfer curves during the reduction process of the polymer (from now on called "*off*" curves) and the oxidation process ("*on*" curves). In Figure 1, the I_{DS} *vs.* V_G curves (Figure 1B) and the first derivative of the transfer curve that represent the transconductance ($g = dI_{DS}/dV_G$) of the channel with the applied gate potential (Figure 1C) are shown. Then, three different parameters were determined, which will be employed in the next sections to monitor sensing processes. The first one, the threshold voltage (V_{TH}), that represents the minimum potential required to oxidize the polymer (and to inject charge carriers), was obtained directly from the transfer curve by fitting the linear region and extrapolating this line to the potential value at which I_{DS} = 0 mA. The maximum transconductance, g_{max}, and the gate potential at which $g = g_{max}$ ($V_{G,gmax}$) were determined from the first derivative as shown in Figure 1B. The latter represents the potential at which the current has the maximum response to the change in the applied gate potential and, therefore, corresponds to the V_G value at which the OECT signal in terms of I_{DS} has the greatest sensitivity to changes in the effective gate voltage.

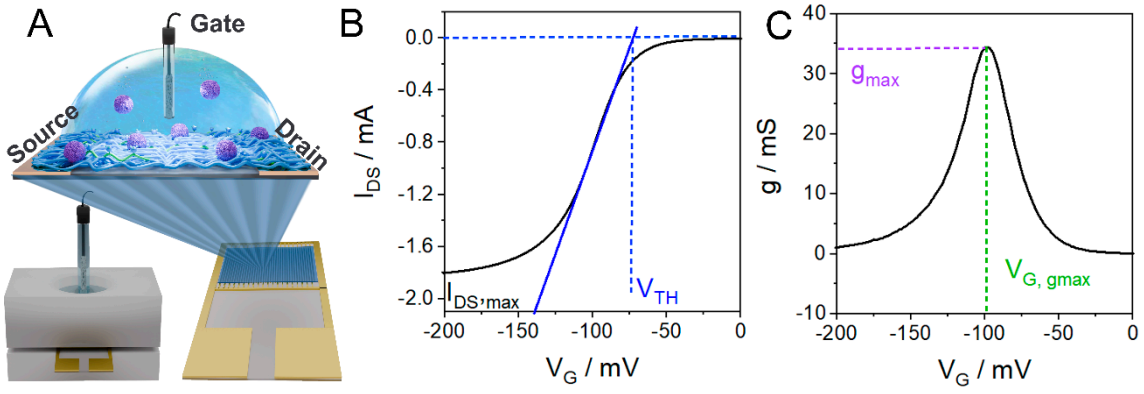

Figure 1. (A) Scheme of the cell and the interdigitated electrodes employed for the measurements shown in this work. (B) Transfer curve of a PANI-based OECT and representation of the determination of the threshold voltage, V_{TH}. (C) Derivative of transfer curve and representation of the determination of the maximum transconductance value, g_{max}, and the maximum transconductance potential, $V_{G,gmax}$.

 doi:10.20944/preprints202512.0526.v1

3.2. Limitations of Traditional OECT Measurements and Introduction to Continuous Cycling Methodology (CCM)

When using OECT-based technology for the development of biosensing devices, determining and controlling the characteristic parameters g, V_{TH} and $V_{G,gmax}$, is critical. In particular, the focus is on obtaining transistors with high values of g (high sensitivity to V_G modulation) [50,54] with low values of $V_{G,gmax}$ and V_{TH} to avoid polymer degradation or parasitic electrochemical reactions [55,56]. To this end, much attention has been paid to the design of channel and gate materials with optimized properties that also allow the incorporation of biomolecules in non-denaturing environments [10,69,70]. Then, the challenge relies on transducing the biochemical events occurring at the channel or gate surface of the OECT into reproducible electrical signals. In many cases, the detection mechanism is based on changes in the interfacial potential due to the adsorption of macromolecules through biorecognition events [71] or due to changes in the external solution properties such as pH, ionic strength or counterions flux, generated by biochemical reactions [66,72]. In all cases, these changes in the physicochemical properties of the gate or channel electrodes lead to changes in the OECT characteristic parameters that can be used as electric signals to monitor sensing events [28,72].

However, the evolution in time of these parameters during the detection measurement is not commonly used to follow the process in real time. In fact, in many works, the measurement of the transfer curves and the determination of the V_{TH}, $V_{G,gmax}$ or g parameters are evaluated before the sensing event occurs and in some cases after analyte addition, but the real-time monitoring of these parameters during the interaction of the analyte with the OECT is not usually performed. Instead, the detection signal is obtained by measuring the variation of I_{DS} at a constant V_G [29,36,40,73,74]. Although this methodology has been successfully employed for the detection of several analytes, it misses out relevant information and may have some limitations and issues associated. In this section, we will illustrate some of these issues and explore the potential of the continuous cycling methodology proposed here to overcome them by using the response of OECTs based in two of the most widely employed conducting polymers in the construction electrochemical devices: poly(3,4-ethylenedioxythiophene) (PEDOT) [75] and polyaniline (PANI) [76–80].

In the first place, choosing a constant V_G to perform current monitoring is not trivial. On one hand, the applied V_G must lie within a potential range with high transconductance. However, determining the optimal value of V_G to perform the measurement is not easy since, for transistors based in organic channel materials, the relationship between the output current of the device with the applied potential depends on several factors. For instance, the electrochemical response of polymers may have associated hysteresis (Figure 2A) [81]. That is, even sweeping at low sweep rates, the *off* and *on* curves have different responses. For this reason, when applying a constant gate potential, the obtained I_{DS} will depend on the previous state of the polymer. To illustrate this, Figure S1A shows the response of a PEDOT-PAH transistor at different sweep rates (v), where the shift of the curves towards more positive gate potentials as v increases can be observed, which is characteristic of mixed conduction polymer systems. For v values lower than 20 mV s^{-1} (Figure S1B), the "*off*" curve (corresponding to the reduction process) shows the same profile, independently of the scan rate, showing that below 20 mV s^{-1} the change in the applied potential is slow enough to allow the polymer to reach the equilibrium state and there are no associated diffusion phenomena that deform the electrochemical response. However, the "*on*" curve shifts with the scan rate to lower gate values due to other phenomena that may be associated with restructuring of the polymer chains, generating a hysteresis in the current response, even at very low values of v. As a consequence, the current signal at a given gate potential depends on the initial state of the polymer. Figure 2B shows the I_{DS} response of a PEDOT-PAH transistor measured at the same V_G value (V_G = 225 mV), obtained from different initial states of the polymer: off-limit (fully reduced), on-limit (fully oxidized), and open circuit potential (OCP). It can be observed that the changes in the output current depend on the initial state of the polymer, even when they were measured at the same constant gate potential.

This effect is even more notorious for PANI-based OECTs, for which the hysteresis in the response yields a difference of 150 mV between the "*on*" and "*off*" curves even at very low scan rates

 doi:10.20944/preprints202512.0526.v1

as 2 mV s^{-1} (Figure 2C). In this case, the initial state of the polymer has a very important role in the current response of the transistor. In Figure 2D, the I_{DS} measured at a constant V_G is shown, where the difference in the output current depending on the initial state of the polymer can be seen. In this experiment, initial gate potentials of 100 mV or -450 mV were applied during 3 min, to fully reduce or oxidize the polymer respectively. Next, a V_G = -250 mV was set and an output current of -0.57 mA was obtained for the experiment where the initial potential was -100 mV and a current of -0.90 mA when the initial potential was -450 mV. This means that, if the polymer was initially oxidized, applying a constant value of -250 mV yields the polymer in a completely "*on*" state with low transconductance. Therefore, a sensing event occurring in the gate electrode that generates a shift in the transfer current will not have a significant effect on the output current. On the contrary, if the polymer was initially reduced, applying a V_G of -250 mV will lead the polymer in a state of high transconductance, yielding to a great sensitivity towards analyte detection. A similar effect, but in the opposite direction occurs at V_G=-150 mV. When the polymer was initially oxidized, applying a V_G of -150 mV generates a state of high transconductance in the polymer (I_{DS} = 0.3 mA), while if the polymer was initially reduced, the current is practically null, and therefore, a sensing event will not be detected. Then, to choose the proper potential to monitor a sensing event, a very thorough study of the polymer behavior and a precise control of its redox state before initiating the measurement is required, and even then, any change in the external media or modification of the polymer surface may change the result.

To show how this may affect a sensing experiment, we monitored the change in the signal of a PANI-based OECT upon the addition of NaOH. The change in the external pH generates changes in the current response of the OECT, since the electrochemical response of PANI strongly depends on the pH. This is the case of many organic composites employed as channel materials in the construction of OECTs, and is often harnessed to monitor sensing events involving enzymatic reactions that generate acidic or basic products. In Figure 2E, the I_{DS} *vs.* V_G profiles of a PANI-based OECT are shown before (blue) and after (purple) the addition of NaOH. A shift of the transfer curves to higher V_G and a decrease in the maximum current, $I_{DS,max}$ can be observed. Next, we choose a V_G potential in the high transconductance region to perform the monitoring of the change in the solution pH using the traditional chronoamperometry methodology, and evaluate the influence of the initial state of the polymer in the resulting signal. To this end, initial potentials of 100 mV or -450 mV were applied during 3 min, and then changed to -250 mV while the I_{DS} was recorded. Next, NaOH solution was injected to change the solution pH (25 µl of a 20 % p/V NaOH were added to a total cell volume of 600 µL of 1 M HCl solution). In Figure 2F, it can be observed a marked increase in the current when the NaOH solution is added, as a consequence of the shift of the transfer curve to higher V_G values, for the case that the previous state of the polymer was fully reduced. However, for the experiment performed with the polymer initially oxidized, there is no appreciable change in the current with the addition of NaOH. The same experiment was performed at -150 mV, where the opposite behavior was found: when the initial state of the polymer was fully oxidized, a marked change in the current was observed upon NaOH solution addition. On the contrary, if the initial state was fully reduced, a very small current was observed, and no changes were appreciated due to pH change (Figure S2). These results show the complexity of selecting a V_G value to perform a detection measurement and the different variables that may affect the result.

 doi:10.20944/preprints202512.0526.v1

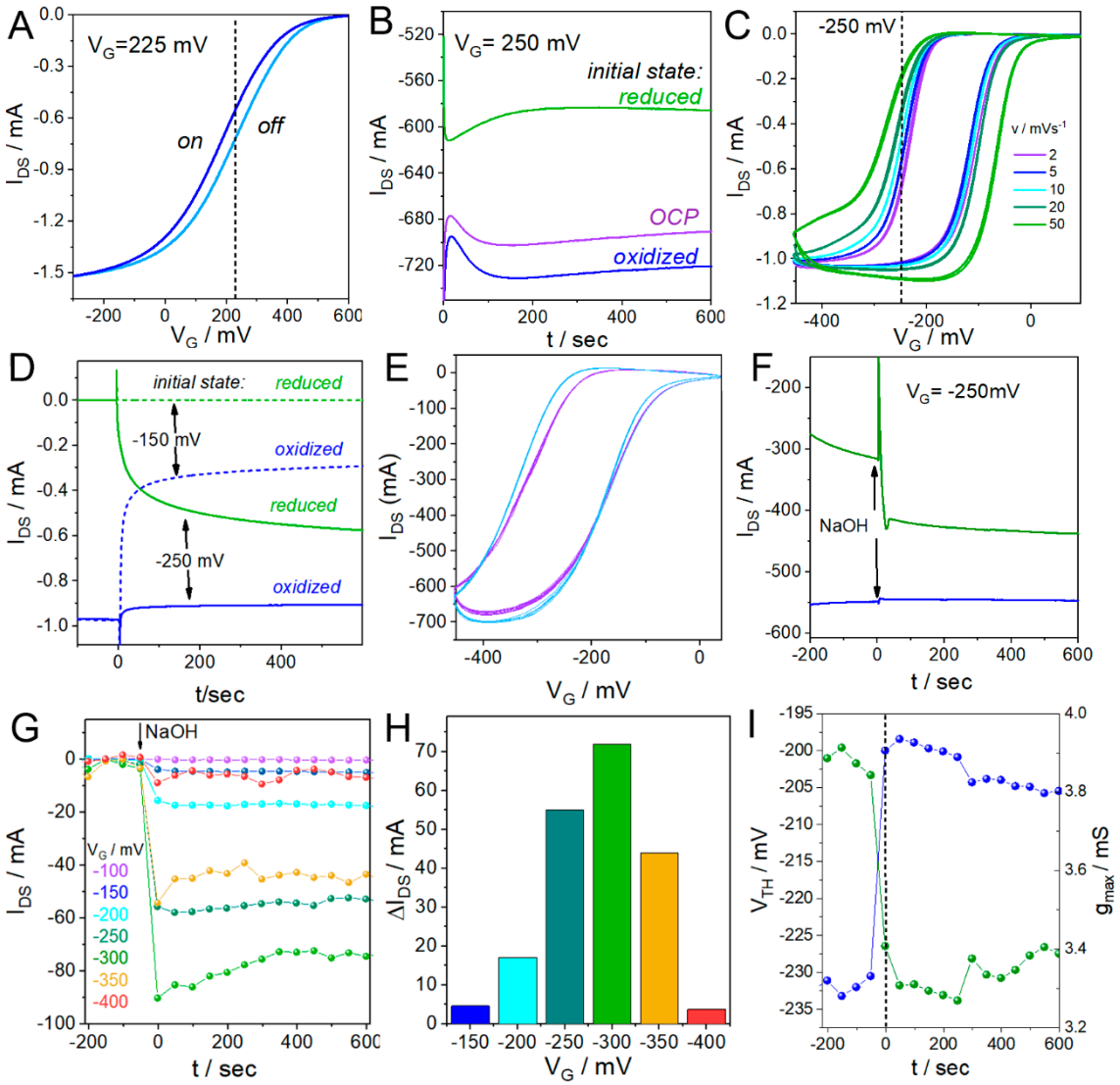

Figure 2. (A) Transfer curve of a PEDOT-PAH -based OECT in 0.1 M KCl at 10 mV s^{-1} and (B) I_{DS} time evolution at V_G=225 mV obtained from three different initial states. (C) PANI-based OECT transfer curves at different scan rates and (D) I_{DS} response at two fixed V_G values: -250 mV (solid lines) and -150 mV (dash lines). (E) Transfer curves of a PANI film in HCl 1M before (blue) and after (purple) the addition of NaOH. (F) Time I_{DS} response of a PANI OECT upon NaOH addition at V_G=-250 mV. (G) Reconstructed I_{DS} *vs.* time response obtained with CMM for different V_G values using the transfer curves shown in (E) and (H) I_{DS} changes as a function of V_G. (I) Time evolution of V_{TH} and g_{max} parameters obtained from the transfer curves shown in (E).

In this context, the CCM proposed here allows overcoming this issue as well as obtaining more information about the processes occurring on the OECT. In this method, the entire transfer curves are continuously recorded during the sensing experiment, and therefore the changes in I_{DS} are registered at all the V_G values within the potential range of the transfer curve. Then, the I_{DS} as a function of time profiles can be reconstructed at each V_G, allowing to choose the value that yields the greatest amplitude of the current change. In Figure S3, the reconstructed values of I_{DS} at different V_G values obtained from only one experiment employing CCM in the same conditions of those employed in the traditional chronoamperometry measurements are shown, for the "*on*" curves (Figure S3A) and the "*off*" curves (Figure S3B). In Figure 2G,H, the changes in the current, ΔI_{DS}, obtained by subtracting a linear baseline to the I_{DS} *vs.* time curves are shown for the "*on*" curves (the analogous results for the "*off*" curves are shown in Figure S4 and the details of the procedure for subtracting the baseline are given in section S4). It can be observed that the amplitude of the current change upon the addition of NaOH depends on the V_G analyzed. Then the potential value that has the greatest sensitivity can be

 doi:10.20944/preprints202512.0526.v1

selected. In addition, the evolution in time of the other parameters can be obtained from the shifts in the transfer curves and their derivatives (transconductance curves shown in Figure S5). In Figure 2I and Figure S6, the changes in V_{TH}, g_{max} and $I_{DS,max}$ are shown, demonstrating that these parameters can also be employed in the monitoring of a sensing event. Moreover, the reconstruction of the I_{DS} *vs.* time profiles from the "*off*" (Figure S4), shows that the change in the current has different behaviors depending on the potential region analyzed. For the potential range V_G > -150 mV, there is an increase in the current (in absolute value) with the addition of NaOH, while for V_G values below -200 mV, there is a decrease in the signal. This can be explained by taking into account two features of the electrochemical response of the polymer. On one hand, there is a well-known change of PANI redox potential with pH increase [82], that leads to a shift in the transfer curves to higher gate potential values. On the other hand, as the pH increases, there is a decrease in PANI conductivity and therefore in the transconductance and maximum current values. Because of these coupled phenomena there is an intersection of the transfer curves that yields different behaviors of the current depending on the potential region analyzed. These results emphasize the relevance of having available the entire transfer curves and monitoring the evolution of the different parameters to understand the phenomena causing the signal in the transistor.

Another problem that arises from measuring at a constant V_G value is that the polarization of the channel and the gate electrode could lead to parasitic reactions, generating a component associated to these processes in the OECT signal. Due to this fact, the time required to achieve the stabilization of the device response as well as the presence of a drift in the transistor signal will depend on the V_G employed. To exemplify this, Figure S7A shows the evolution of the signal of a PEDOT-PAH transistor during the first 20 min after applying a constant V_G. This response was measured for four different V_G values in the potential region of high transconductance, and were expressed as I_{DS} - $I_{DS,t=20min}$ for the sake of comparison. It can be observed that the time to reach a stable signal and the drift in the signal depend on the applied potential. In this regard, sweeping the gate potential between the *on* and *off* states avoids polarization preventing parasitic reactions that add non desirable components to the device signal. Then, the time required to stabilize the output signal does not have an important variation with the V_G chosen to monitor the evolution of the current. In Figure S7A, the reconstructed I_{DS} at a function of time curves obtained with the CCM are shown at different V_G values and compared with the traditional I_{DS} measurements at constant V_G. It can be appreciated that, with this methodology, the time to reach stabilization as well as the drift in the signal is independent of the chosen potential.

Moreover, the analysis of other parameters, such as the threshold voltage, can contribute to elucidate the origin of the drift in a measurement and in some cases, to mitigate its effect. For instance, drifts often originate in the degradation processes of the polymer or their detachment from the substrate. In this case, the OECT current progressively decreases and separating this contribution from the change in the current due to an actual sensing event can be a challenge. However, it is interesting to note that the threshold voltage does not necessarily change due to this effect. In Figure S7B, it is shown the evolution of the transfer curves of a PEDOT-PAH transistor that suffers degradation. A decrease in the maximum current of the OECT and a drift in the I_{DS} at $V_G = V_{G,gmax}$ as a function of time can be appreciated (Figure S7C). However, in Figure S7D, it is shown that the V_{TH} remains constant in time. In the following sections, we show how this strategy can be harnessed to detect the presence of an analyte through the monitoring of V_{TH}, in conditions in which the current does not show a clear response.

All these results together, demonstrate the relevance of determining the different OECT parameters and the potential of monitoring them to improve the performance of OECTs in biosensing measurements. We believe that having all this data available from each experiment is a key factor towards reproducibility and a better understanding of the physicochemical processes that take place during detection events. In the following sections, we will show examples of the application of CCM for the detection of different analytes, going from the monitoring of the adsorption of polyelectrolytes

 doi:10.20944/preprints202512.0526.v1

and enzymes into polymeric substrates, to the biosensing of glucose and urea through biocatalytic reactions.

3.3. CCM Applied to Polyelectrolyte Adsorption Monitoring with OECTs

In this section, we show the monitoring of the adsorption of a polyelectrolyte (poly-styrenesulfonate, PSS) on the PEDOT-PAH channel surface through the analysis of the different parameters mentioned above. The adsorption of this macromolecule onto the PEDOT-PAH surface has been previously studied and it is driven by the electrostatic interaction between the negatively charged PSS and the positive charge of the channel surface endowed by the amino groups of the polyallylamine.

To this end, the OECT I_{DS} response was recorded while the gate potential was swept between -200 mV and 600 mV in KCl 0.1 M at 20 mV s^{-1} under flow conditions. Then, a 1 mg mL^{-1} PSS in 0.1 M KCl solution was injected for 40 min and then rinsed with KCl. In Figure 3A, the change in the transfer response is shown for the "*off*" curves (the *on* curves were separated and shown in the SI for the sake of clarity, Figure S8). A shift of the curves to higher gate values can be observed. This effect can be also appreciated in Figure 3B, which shows the transconductance *vs.* V_G for the transfer curves of Figure 3A. Then, the V_{TH} was calculated from each curve, and plotted *vs.* time, as can be seen in Figure 3C. A rapid increase in V_{TH} as the charged macromolecule is deposited can be observed. The increase in the gate potential required to oxidize the polymer when PSS is adsorbed, is related with the incorporation of a negative dopant in the PEDOT-PAH matrix, that stabilizes the positive carriers of the polymer. This effect can also be monitored by following the increase in $V_{G,gmax}$ as it is shown in Figure S9A. In addition, Figure 3D shows the g_{max} values as a function of time, at which a decrease of this parameter as PSS is deposited on the surface can be appreciated. Next, we continued with the reconstruction of the I_{DS} *vs.* time profiles usually used to monitor these processes at different constant V_G values. Figure S10 shows the I_{DS} time evolution at different potentials where it can be observed that the output signal of the device depends on the selected V_G, as expected. However, some interesting information arises from the comparison of the changes in the current at the different V_G. Figure 3E,F, show the changes in the current at each value V_G obtained by subtracting a lineal baseline corresponding to the current before the injection (see Figure S11 for more details), ΔI_{DS}, which is the typically used analytical parameter with OECTs (these results were obtained using the "*off*" curves, the ones obtained with the "*on*" curves are shown in Figure S12A). The maximum amplitude of the change in the signal is observed at the potential corresponding to the maximum transconductance of the polymer (380 mV). However, it is interesting to note that a different result is obtained when analyzing the relative changes in the current or normalized current response, $\%\Delta I_{DS}$, which is the ratio between the current change upon analyte addition and the initial current value before the injection ($\%\Delta I_{DS}=100\Delta I_{DS}/I_{DS,0}$). This parameter is often employed to compare the performance of different transistors [74] and does not necessarily have the greatest amplitude in the $V_{G,gmax}$. In fact, for the case of PSS adsorption on the PEDTO-PAH-based OECT, the magnitude of the relative current changes increases with V_G, reaching values of 66% for a V_G= 660 mV, compared with a 24% change at $V_{G,gmax}$ (Figure S12B). These differences will depend on each specific system and are not easy to predict, therefore having all data available allows selecting the optimal potential to perform the analysis and obtain the signal of greatest amplitude and then having a fair comparison between different devices.

In addition, we compared the OECT response obtained with the CCM with SPR results, to evaluate the influence of the methodology in the kinetic profile of the reconstructed curves. To this end, a PEDOT-PAH modified Au-SPR substrate was employed to follow the change in the sensorgram during the injection of 0.1 mg mL^{-1} PSS in 0.1 M KCl solution (same conditions of those employed for the OECT measurements). In Figure S13, the comparison between the results obtained with the two techniques are shown. In Figure S13A, the SPR response is compared with the change in V_{TH} upon PSS adsorption, calculated as $\Delta V_{TH}=V_{TH}-V_{TH,0}$, where $V_{TH,0}$ is the threshold potential before PSS injection, and Figure S13B, shows the comparison with the I_{DS} profile at V_G=380 mV,

 doi:10.20944/preprints202512.0526.v1

corresponding to the maximum transconductance potential. In both cases, a remarkable match of the kinetic profiles of the reconstructed responses with the SPR profile can be observed. This shows that CCM allows precise time monitoring of the processes.

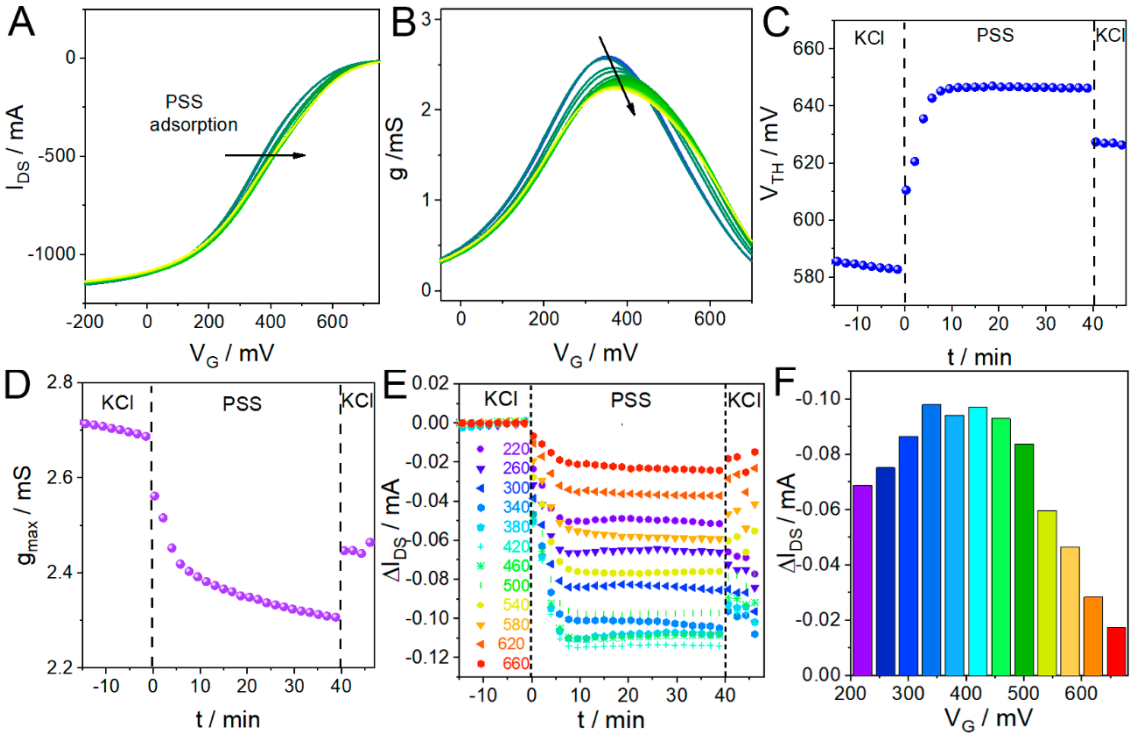

Figure 3. (A) Shift of the PEDOT-PAH transfer curves during PSS adsorption. (B) *g vs.* V_G curves obtained by deriving transfer curves in (A). (C) V_{TH} and (D) g_{max} time evolution obtained from the curves in (A) and (B), respectively. (E) ΔI_{DS} time evolution during PSS deposition at different V_G values, and (F) representation of the current changes as a function of V_G. All shown data was obtained from the *"off"* curves, see SI for the analysis of the *"on"* curves (Figure S12).

3.4. CCM Applied to Enzyme Adsorption Monitoring with OECTs

The anchoring of urease and glucose oxidase on PEDOT-PAH OECTs have been previously reported [66,67,71]. These enzymes are negatively charged in aqueous media at pH 7.4. Then, due to electrostatic interactions, they are adsorbed on the protonated polymeric surface. In previous works, we have shown the capability of OECTs to monitor protein deposition on PEDOT-PAH films through the changes in the current signal of the device. Here, we report the monitoring of the adsorption of urease and glucose oxidase on the OECT channel by following the time evolution of V_{TH}, $V_{G,gmax}$ and g_{max}, showing the advantages of this analysis methodology.

The integration of enzymes onto PEDOT-PAH films was performed similarly to polyelectrolyte adsorption. Briefly, under flow conditions, a solution of 10 mM KCl was injected, and the I_{DS} was recorded while the potential was swept between 0 and 800 mV at 10 mV s^{-1}. Then, 1 mg mL^{-1} urease in 10 mM KCl was injected for 32 min followed by rinsing with 10 mM KCl. Figure 4 shows the time evolution of g_{max}, V_{TH} and $V_{G,gmax}$. These parameters were obtained from both transfer curves, *"on"* and *"off"*. The transfer curves recorded before and after enzyme deposition (Figure S14A) show a clear shift toward lower gate potentials. This variation is also reflected in the time evolution of g_{max}, V_{TH} and $V_{G,gmax}$ as it can be appreciated in Figure 4A–C. In previous works, such behavior has been attributed to changes in the impedance at the polymer/electrolyte interface due to enzyme attachment on the channel surface [67]. Overall, it is interesting to note that all studied parameters are suitable for monitoring the enzyme integration process.

A similar analysis was performed using Glucose Oxidase (GOx) instead of urease (Figure S15). In this case, the enzyme injection was for 29 min, and the behavior of the parameters was opposite to

 doi:10.20944/preprints202512.0526.v1

urease incorporation. In particular, the increment in the conductivity of the channel due to the anchoring of the GOx was attributed to stabilization of the positive charge carriers of the polymer by the negative charges of the enzyme, similarly to the behaviour observed for PSS adsorption [71], corroborating the capability of this strategy for monitoring enzyme integration (See Figure S15).

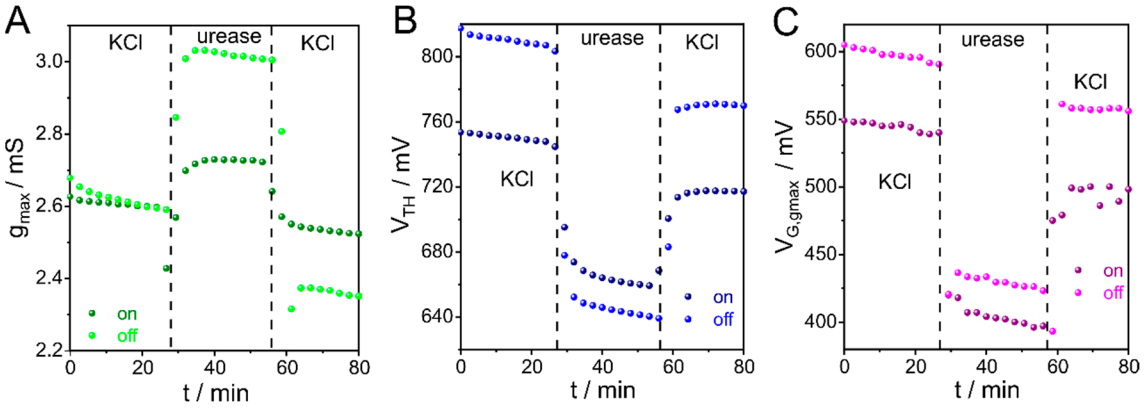

Figure 4. Time evolution of the (A) g_{max}, (B) V_{TH} and (C) $V_{G,gmax}$ during urease adsorption. V_{DS} = -50 mV, pH 7.4.

Likewise, a similar approach of that shown above for PSS was applied here to compare the OECT response with the SPR signal during urease deposition. In this case, a PEDOT-PAH modified Au-SPR substrate was employed to follow the change in the sensorgram during the injection of 1 mg mL^{-1} of the enzyme in 10 mM KCl solution. Figure S14B–D shows the SPR response compared with the change in V_{TH}, $V_{G,gmax}$ and g_{max}, upon urease adsorption. In all cases, the reconstructed kinetic profiles exhibited a notable correspondence with the SPR sensorgram. These results verify the capability of the CCM to monitor the adsorption process in time with high precision.

3.5. CCM Applied to the Biosensing of Catalytic Reaction with OECTs

Urease catalyzes the hydrolysis of urea into ammonia and carbon dioxide, yielding an increase in the local pH. The catalytic response of enzyme adsorbed PEDOT-PAH OECTs is shown in this section. For urea detection, the urease modified OECT mentioned above was exposed to increasing concentrations of urea, from 100 µM to 5 mM in 10 mM KCl, pH 7.4, injected under flow conditions. Transfer curves were recorded between 0 and 850 mV at 10 mV s^{-1} and as shown in Figure S16, they exhibit a shift toward higher gate potentials. As a result, there is an increase in V_{TH}, $V_{G,gmax}$ and g_{max} parameters as a function of time (Figure 5A–C). In previous works, it was stated that the shift toward higher gate potentials upon pH increase arises from the deprotonation of PAH amino groups, leading to stabilization of the PEDOT channel positive charge carriers [67].

Figure 5D presents the V_{TH} and $V_{G,gmax}$ as functions of urea concentration. The plot shows an increase of these parameters throughout the entire concentration range studied and a good match of the profiles, suggesting that both parameters can be equally employed for urea detection. A similar behavior was observed with $\%\Delta I_{DS}$ and $\%\Delta g_{max}$ parameters (Figure 5E), that represent the relative change of I_{DS} and g_{max}, respectively ($\%\Delta g_{max}$ was computed as $\%\Delta g_{max} = 100(g_{max} - g_{max,0})/g_{max,0}$ and $\%\Delta I_{DS}$ was evaluated at a constant V_G corresponding to the $V_{G,gmax}$).

In addition, we reconstructed the I_{DS} *vs.* time profiles under different constant V_G values (Figure S17A). As observed for PSS, time evolution of I_{DS} at different potentials shows that the device output signal depends on the selected V_G. From the analysis of the ΔI_{DS} obtained at the different V_G, it can be seen that the maximum signal amplitude is also reached at the gate potential corresponding to the maximum transconductance of the polymer (306 mV) (Figure 5F). On the other hand, the relative changes in the normalized current response, $\%\Delta I_{DS}$, increases with V_G (Figure S17B), similar to that observed for the monitoring of macromolecule adsorption. These results reinforce the importance of

 doi:10.20944/preprints202512.0526.v1

considering the complete set of experimental data in order to identify the gate potential that maximizes the signal amplitude and ensure a consistent and reliable comparison between devices.

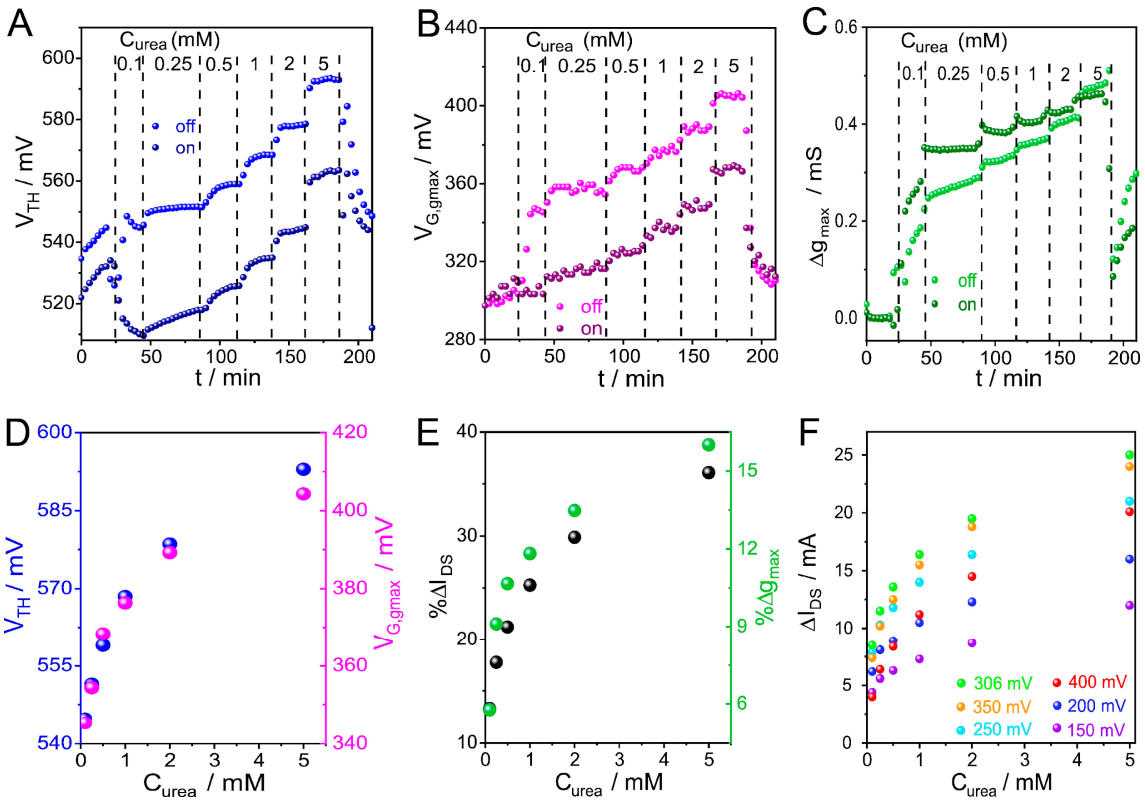

Figure 5. Time evolution of the (A) V_{TH}, (A) $V_{G,gmax}$ and (C) g_{max} along the injection of increasing concentrations of urea. (D) V_{TH} and $V_{G,gmax}$ as a function of concentration. (E) Percentual change of I_{DS} and g_{max} as function of concentration. (E) Percentual change of I_{DS} as function of concentration evaluated at constant and variable V_G. V_{DS} = -50 mV, pH 7.4. (F).

Furthermore, we have also evaluated the enzymatic detection of glucose through the different parameters with a PEDOT-PAH OECT modified with GOx, showing that the CMM can be successfully employed for the monitoring of this analyte (Figure S18). However, some worth mentioning results emerged from an experiment performed with a modified electrode channel that suffered degradation, losing polymeric material during the sensing measurement and therefore decreasing the current signal. When this kind of issue appears in a sensing measurement, the I_{DS} shift cannot be clearly associated either to the degradation or to the molecular reaction that occurs in the polymeric surface. For the case of glucose sensing, its decomposition into gluconic acid and hydrogen peroxide in the presence of GOx results in a decrease of current, behavior attributed to the medium acidification. Therefore, in this case, both the sensing event and the degradation process yield a decrease in the current and separating one contribution from the other is not possible using only the current signal. In this context, a possible solution is to use parameters that do not strongly depend on the polymer mass to follow the enzymatic reaction. Figure 6 shows the behavior of a PEDOT-PAH OECT that is degrading while the glucose detection is being monitored (glucose was injected from 0.5 to 10 mM in 10 mM KCl at pH 7.4). The evolution of the transfer curves (Figure 6A) shows the decrease of I_{DSmax} while the glucose concentration increases, which involves an obstacle to monitor the glucose detection by the recording of I_{DS} at a constant V_G (Figure 6B). In fact, for values higher to 5 mM, it is not possible to correlate current with concentration and it seems that the enzyme saturation was reached. Otherwise, if we use V_{TH} to follow the glucose detection (Figure 6C) it is possible to sense concentrations beyond 5 mM. This issue can be corroborated in the comparison between the relative change of current and the change of V_{TH} as function of concentration shown in

 doi:10.20944/preprints202512.0526.v1

Figure 6D. While the %ΔI_{DS} appears to reach a plateau at 5 mM of glucose, the ΔV_{TH} is continuously increasing until 10 mM glucose.

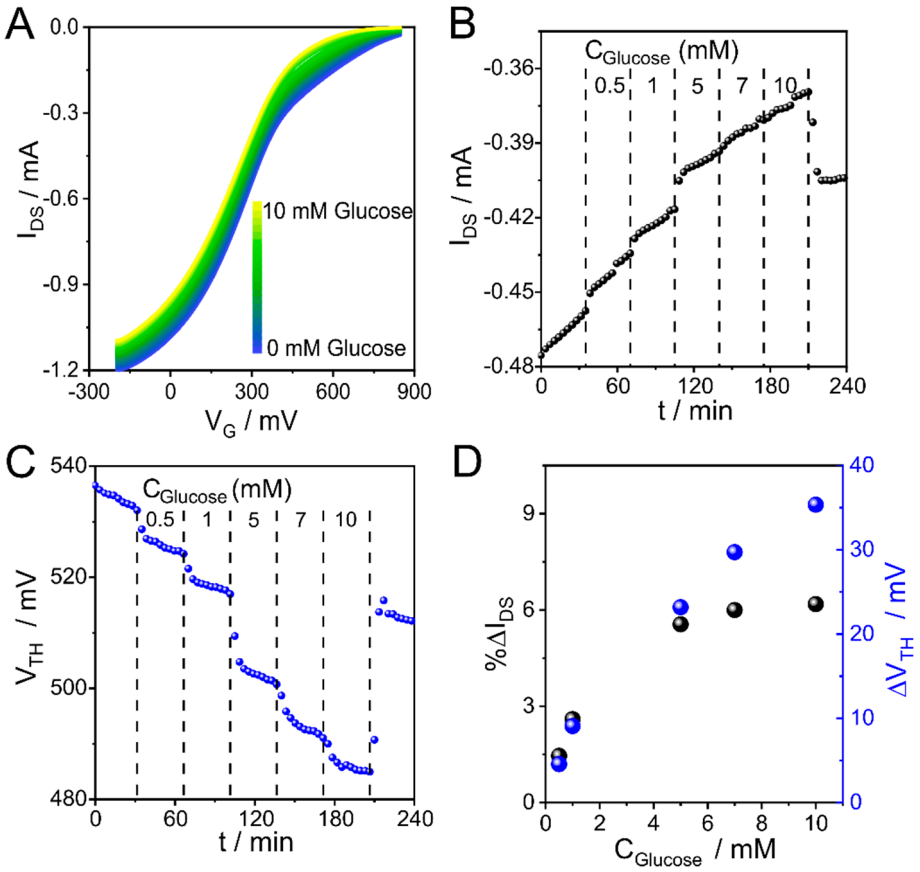

Figure 6. (A) I_{DS} *vs.* V_G *"on"* curves for glucose sensing with a GOx-adsorbed PEDOT/PAH OECT in 10 mM KCl, pH 7.4 (B) Time evolution of the I_{DS} and (C) V_{TH}. (D) Percentual change of I_{DS} and change of V_{TH} as function of glucose concentration.

3.6. Sensing Rapid Processes with CCM

In previous sections it was shown the capability of CCM for monitoring the time adsorption of macromolecules on the OECT channel surface and the good correlation between the kinetic profile obtained by this technique and those obtained by the reference SPR technique. However, when studying the evolution of processes over time, the frequency of data determination is a critical parameter. In this regard, because of the time that takes cycling the polymer between the *"on"* and *"off"* states, the amount of points obtained in the reconstructed curves may be less than desired. In this context, reducing the potential window in which the polymer is cycle can be an easy way to overcome this potential issue. In this section, we prove this concept by reducing the potential range during the detection of glucose. To this end, a GOx-adsorbed PEDOT-PAH OECT was used to monitor a solution of 5 mM glucose in 10 mM KCl. First, the complete transfer curves (Figure 7A) were recorded while the solutions were injected (10 mM KCl followed by 5 mM Glucose in 10 mM KCl). The potential was swept from -200 *("on"* state) to 850 mV (*"off"* state). Next, using the same OECT, the experiment was repeated by setting the V_G limits shown in the orange box, from 350 to 550 mV, at the same conditions as previously used (Figure 7B). The polymer state is not the same when the scan limits change. This issue can be attributed to the doped degree that is reached when it is completely oxidized and then reduced. Since the polymer does not work under the same initial and final conditions, a different time evolution of I_{DS} is expected (Figure S19). Although there is noticeable variation in I_{DS}, the reduction of the window of V_G does not modify the relative change of I_{DS}, (see Figure 7C). In both cases, the complete and the short scan, a shift around 27% of relative I_{DS}

 doi:10.20944/preprints202512.0526.v1

was reached. A noteworthy point is that the short-cycle scan allows tracking the kinetic profile of the biosensing process with significantly more precision than the complete-cycle scan.

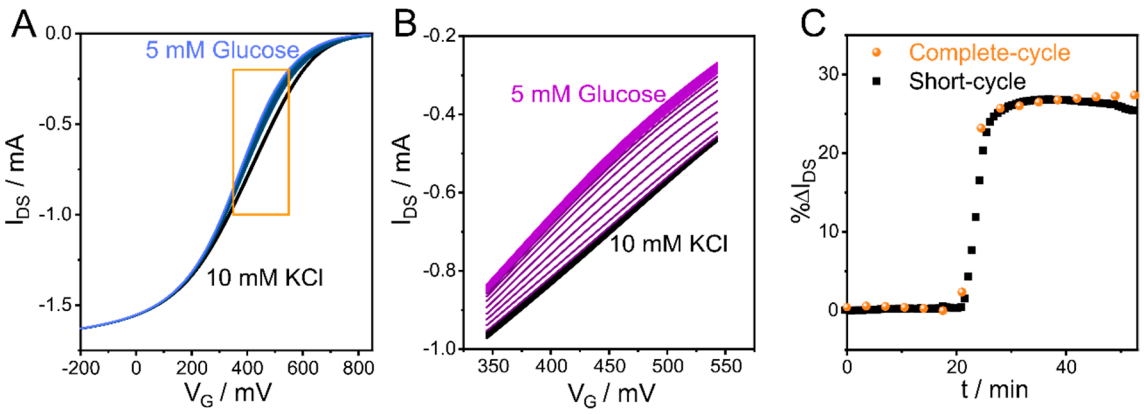

Figure 7. I_{DS}-V_G curves for 5 mM glucose sensing with a GOx-adsorbed PEDOT/PAH OECT in 10 mM KCl, pH 7.4 in (A) complete and (B) short-cycle scan. And (C) $\%\Delta I_{DS}$ time evolution during glucose sensing with different V_G windows, curves reconstructed at V_G = 435 mV.

4. Conclusions

A novel methodology for measuring with OECTs and to analyze the obtained data designed to improve sensors' performance was presented. This methodology is based on the continuous cycling of the transistor channel by scanning the gate potential during the sensing experiments enabling the monitoring of the processes occurring at the OECT electrodes through multiple parameters simultaneously. It was proved that the time monitoring of V_{TH}, $V_{G,gmax}$ and g_{max} parameters can be employed to sense changes in pH solution as well as the adsorption of macromolecules on the channel surface with transistors based on PANI and PEDOT. In addition, the reconstruction of the I_{DS} profiles as a function of time at constant V_G, can be performed at multiple V_G values allowing to select the optimum gate potential to analyze the experiment. This represents a major improvement compared with traditional measurements of I_{DS} at constant V_G, since it allows choosing the analysis conditions that yields the greatest sensitivity in the signal response as well as avoiding the issue of gate polarization that leads to parasitic reactions. In addition, the extra information provided by the determination of multiple parameters leads to a better understanding of the physicochemical processes occurring at the gate and channel electrodes. In this work, the CCM was successfully applied for the time monitoring of polyelectrolyte and enzyme adsorption and for the detection of urea and glucose through enzymatic reactions. However, we believe it could be easily extended to other systems of interest, making this methodology a significant contribution for the development of devices based on OECTs technology.

Supplementary Materials: The following supporting information can be downloaded at: https://www.mdpi.com/article/doi/s1, Figure S1: Transfer curves at different scan rates in a PEDOT-PAH OECT, Figure S2: NaOH sensing with a PANI OECT, Figure S3: Reconstructed time evolution of I_{DS} curves in a PANI OECT at different V_G, Figure S4: ΔI_{DS} as a function of time for the *"off"* curves in Figure 2C, Figure S5: Transconductance of the PANI OECT obtained from deriving curves in Figure 2C, Figure S6: V_{TH}, g_{max} and $I_{DS,max}$ values upon NaOH obtained using CCM from the data in Figure 2E, Figure S7: Current profile a PEDOT-PAH transistor in KCl during the first 20 min of the stabilization. Figure S8: *"On"* transfer curves and *g vs.* V_G profiles for a PEDOT-PAH-based OECT during PSS deposition, Figure S9: Time evolution of V_{TH}, $V_{G,gmax}$ and g_{max} during PSS adsorption, Figure S10: Reconstructed I_{DS} *vs* time profiles using CCM at different potentials, Figure S11: Example of baseline subtraction, Figure S12: ΔI_{DS} and $\%\Delta I_{DS}$ at different V_G, Figure S13: Comparison of the performance of SPR and OECT techniques for the monitoring of PSS deposition, Figure S14: Transfer curves and comparison of the performance of SPR and OECT techniques for the monitoring of urease adsorption, Figure

 doi:10.20944/preprints202512.0526.v1

S15: Time evolution of the V_{TH}, $V_{G,gmax}$ and g_{max} during GOx adsorption, Figure S16: Transfer curves for urea sensing, Figure S17: Time evolution of the I_{DS} and $\%\Delta I_{DS}$ for urea sensing, Figure S18: Time evolution of the V_{TH}, $V_{G,gmax}$ and g_{max} during glucose sensing, Figure S19: I_{DS} time evolution during glucose sensing with different V_G windows.

Author Contributions: Conceptualization, JS, WAM; methodology, JRNR, MMJ, JS; formal analysis, JS; investigation, JRNR, MMJ; data curation, JRNR, MMJ, JS; writing—original draft preparation, MMJ, JRNR, JS; writing—review and editing, OA, JS, WAM; visualization, MMJ, JRNR, JS; supervision, JS, WAM; project administration, OA, WAM; funding acquisition, OA, WAM. All authors have read and agreed to the published version of the manuscript.

Funding: This research was funded by Universidad Nacional de La Plata (PID-X1016), CONICET (PIP 11220210100209CO, PIBAA 2872021010 0870CO), and ANPCyT (PICT-2020-02468, PICT-2020-SERIEA-0356 and PICT-2021-GRFTI-00042).

Data Availability Statement: The original contributions presented in this study are included in the article/supplementary material. Further inquiries can be directed to the corresponding author(s).

Acknowledgments: MMJ and JRNR acknowledge scholarships from CONICET; OA, JS and WAM are staff members of CONICET.

Conflicts of Interest: The authors declare no conflicts of interest.

References

1. Singh, R.; Gupta, R.; Bansal, D.; Bhateria, R.; Sharma, M. A Review on Recent Trends and Future Developments in Electrochemical Sensing. *ACS Omega* **2024**, doi:10.1021/acsomega.3c08060.
2. Baranwal, J.; Barse, B.; Gatto, G.; Broncova, G.; Kumar, A. Electrochemical Sensors and Their Applications: A Review. *Chemosensors* **2022**, *10*, 363, doi:10.3390/chemosensors10090363.
3. Ronkainen, N.J.; Halsall, H.B.; Heineman, W.R. Electrochemical biosensors. *Chem. Soc. Rev.* **2010**, *39*, 1747–1763, doi:10.1039/b714449k.
4. Singh, A.; Sharma, A.; Ahmed, A.; Sundramoorthy, A.K.; Furukawa, H.; Arya, S.; Khosla, A. Recent Advances in Electrochemical Biosensors: Applications, Challenges, and Future Scope. *Biosensors* **2021**, *11*, 336, doi:10.3390/bios11090336.
5. Zhu, C.; Yang, G.; Li, H.; Du, D.; Lin, Y. Electrochemical Sensors and Biosensors Based on Nanomaterials and Nanostructures. *Anal. Chem.* **2015**, *87*, 230–249, doi:10.1021/ac5039863.
6. Gutiérrez-Capitán, M.; Baldi, A.; Fernández-Sánchez, C. Electrochemical Paper-Based Biosensor Devices for Rapid Detection of Biomarkers. *Sensors* **2020**, *20*, 967, doi:10.3390/s20040967.
7. Noviana, E.; McCord, C.P.; Clark, K.M.; Jang, I.; Henry, C.S. Electrochemical paper-based devices: sensing approaches and progress toward practical applications. *Lab Chip* **2020**, *20*, 9–34, doi:10.1039/C9LC00903E.
8. Rivnay, J.; Inal, S.; Salleo, A.; Owens, R.M.; Berggren, M.; Malliaras, G.G. Organic electrochemical transistors. *Nat. Rev. Mater.* **2018**, *3*, 17086, doi:10.1038/natrevmats.2017.86.
9. Zeglio, E.; Inganäs, O. Active Materials for Organic Electrochemical Transistors. *Adv. Mater.* **2018**, *30*, 1800941, doi:10.1002/adma.201800941.
10. Ohayon, D.; Druet, V.; Inal, S. A guide for the characterization of organic electrochemical transistors and channel materials. *Chem. Soc. Rev.* **2023**, *52*, 1001–1023, doi:10.1039/D2CS00920J.
11. Fenoy, G.E.; Marmisollé, W.A.; Knoll, W.; Azzaroni, O. Highly sensitive urine glucose detection with graphene field-effect transistors functionalized with electropolymerized nanofilms. *Sensors & Diagnostics* **2022**, *1*, 139–148, doi:10.1039/D1SD00007A.
12. Piccinini, E.; Fenoy, G.E.; Cantillo, A.L.; Allegretto, J.A.; Scotto, J.; Piccinini, J.M.; Marmisollé, W.A.; Azzaroni, O. Biofunctionalization of Graphene-Based FET Sensors through Heterobifunctional Nanoscaffolds: Technology Validation toward Rapid COVID-19 Diagnostics and Monitoring. *Adv. Mater. Interfaces* **2022**, *9*, 2102526, doi:10.1002/admi.202102526.
13. Vu, C.-A.; Chen, W.-Y. Field-Effect Transistor Biosensors for Biomedical Applications: Recent Advances and Future Prospects. *Sensors* **2019**, *19*, 4214, doi:10.3390/s19194214.

 doi:10.20944/preprints202512.0526.v1

14. Tian, Z.; Zhao, Z.; Yan, F. Organic electrochemical transistor in wearable bioelectronics: Profiles, applications, and integration. *Wearable Electron.* **2024**, *1*, 1–25, doi:10.1016/j.wees.2024.03.002.
15. Piccinini, E.; Allegretto, J.A.; Scotto, J.; Cantillo, A.L.; Fenoy, G.E.; Marmisollé, W.A.; Azzaroni, O. Surface Engineering of Graphene through Heterobifunctional Supramolecular-Covalent Scaffolds for Rapid COVID-19 Biomarker Detection. *ACS Appl. Mater. Interfaces* **2021**, *13*, 43696–43707, doi:10.1021/acsami.1c12142.
16. *Graphene Field-Effect Transistors: Advanced Bioelectronic Devices for Sensing Applications*; Azzaroni, O., Knoll, W., Eds.; VCH-Wiley: Weinheim, 2023; ISBN 3527349901.
17. Ono, T.; Okuda, S.; Ushiba, S.; Kanai, Y.; Matsumoto, K. Challenges for Field-Effect-Transistor-Based Graphene Biosensors. *Materials (Basel).* **2024**, *17*, 333, doi:10.3390/ma17020333.
18. Zeng, X.; Peng, C.; Shi, W.; Hu, S.; Cao, Y.; Wei, H.; Chen, P.; Xia, J.; Ding, J.; Zhang, Y.; et al. An Interlayer Strategy for Low-Voltage Thin-Film Organic Electrochemical Transistors. *Small Methods* **2025**, *9*, doi:10.1002/smtd.202500322.
19. Niu, Y.; Qin, Z.; Zhang, Y.; Chen, C.; Liu, S.; Chen, H. Expanding the potential of biosensors: a review on organic field effect transistor (OFET) and organic electrochemical transistor (OECT) biosensors. *Mater. Futur.* **2023**, *2*, 042401, doi:10.1088/2752-5724/ace3dd.
20. Galliani, M.; Diacci, C.; Berto, M.; Sensi, M.; Beni, V.; Berggren, M.; Borsari, M.; Simon, D.T.; Biscarini, F.; Bortolotti, C.A. Flexible Printed Organic Electrochemical Transistors for the Detection of Uric Acid in Artificial Wound Exudate. *Adv. Mater. Interfaces* **2020**, *7*, 1–7, doi:10.1002/admi.202001218.
21. Decataldo, F.; Grumiro, L.; Marino, M.M.; Faccin, F.; Giovannini, C.; Brandolini, M.; Dirani, G.; Taddei, F.; Lelli, D.; Tessarolo, M. Fast and real-time electrical transistor assay for quantifying SARS-CoV-2 neutralizing antibodies. *Commun. Mater.* **2022**, *3*, 5.
22. Pappa, A.M.; Ohayon, D.; Giovannitti, A.; Maria, I.P.; Savva, A.; Uguz, I.; Rivnay, J.; McCulloch, I.; Owens, R.M.; Inal, S. Direct metabolite detection with an n-type accumulation mode organic electrochemical transistor. *Sci. Adv.* **2018**, *4*, eaat0911.
23. Saraf, N.; Woods, E.R.; Peppler, M.; Seal, S. Highly selective aptamer based organic electrochemical biosensor with pico-level detection. *Biosens. Bioelectron.* **2018**, *117*, 40–46.
24. Takemoto, A.; Araki, T.; Nishimura, K.; Akiyama, M.; Uemura, T.; Kiriyama, K.; Koot, J.M.; Kasai, Y.; Kurihira, N.; Osaki, S. Fully Transparent, Ultrathin Flexible Organic Electrochemical Transistors with Additive Integration for Bioelectronic Applications. *Adv. Sci.* **2023**, *10*, 2204746.
25. Huang, W.; Chen, J.; Yao, Y.; Zheng, D.; Ji, X.; Feng, L.-W.; Moore, D.; Glavin, N.R.; Xie, M.; Chen, Y.; et al. Vertical organic electrochemical transistors for complementary circuits. *Nature* **2023**, *613*, 496–502, doi:10.1038/s41586-022-05592-2.
26. Fenoy, G.E.; von Bilderling, C.; Knoll, W.; Azzaroni, O.; Marmisollé, W.A. PEDOT:Tosylate-Polyamine-Based Organic Electrochemical Transistors for High-Performance Bioelectronics. *Adv. Electron. Mater.* **2021**, *7*, 1–13, doi:10.1002/aelm.202100059.
27. Fenoy, G.E.; Hasler, R.; Quartinello, F.; Marmisollé, W.A.; Lorenz, C.; Azzaroni, O.; Bäuerle, P.; Knoll, W. "Clickable" Organic Electrochemical Transistors. *JACS Au* **2022**, *2*, 2778–2790, doi:10.1021/jacsau.2c00515.
28. Marks, A.; Griggs, S.; Gasparini, N.; Moser, M. Organic Electrochemical Transistors: An Emerging Technology for Biosensing. *Adv. Mater. Interfaces* **2022**, *9*, 2102039, doi:10.1002/admi.202102039.
29. Wang, N.; Yang, A.; Fu, Y.; Li, Y.; Yan, F. Functionalized Organic Thin Film Transistors for Biosensing. *Acc. Chem. Res.* **2019**, *52*, 277–287, doi:10.1021/acs.accounts.8b00448.
30. Koklu, A.; Ohayon, D.; Wustoni, S.; Druet, V.; Saleh, A.; Inal, S. Organic Bioelectronic Devices for Metabolite Sensing. *Chem. Rev.* **2022**, *122*, 4581–4635, doi:10.1021/acs.chemrev.1c00395.
31. Lin, P.; Yan, F. Organic Thin-Film Transistors for Chemical and Biological Sensing. *Adv. Mater.* **2012**, *24*, 34–51, doi:10.1002/adma.201103334.
32. Bernards, D.A.; Malliaras, G.G. Steady-State and Transient Behavior of Organic Electrochemical Transistors. *Adv. Funct. Mater.* **2007**, *17*, 3538–3544, doi:10.1002/adfm.200601239.
33. Kukhta, N.A.; Marks, A.; Luscombe, C.K. Molecular Design Strategies toward Improvement of Charge Injection and Ionic Conduction in Organic Mixed Ionic-Electronic Conductors for Organic Electrochemical Transistors. *Chem. Rev.* **2022**, *122*, 4325–4355, doi:10.1021/acs.chemrev.1c00266.

 doi:10.20944/preprints202512.0526.v1

34. Paulsen, B.D.; Tybrandt, K.; Stavrinidou, E.; Rivnay, J. Organic mixed ionic–electronic conductors. *Nat. Mater.* **2020**, *19*, 13–26, doi:10.1038/s41563-019-0435-z.
35. Aftab, S.; Zhou, J.; Cheng, Y.; Zhao, D.; Chen, H.; Huang, W. Functional gate modification for OECT-based sensors. *Mater. Today Chem.* **2025**, *48*, 102933, doi:10.1016/j.mtchem.2025.102933.
36. Fan, J.; Forero Pico, A.A.; Gupta, M. A functionalization study of aerosol jet printed organic electrochemical transistors (OECTs) for glucose detection. *Mater. Adv.* **2021**, *2*, 7445–7455, doi:10.1039/D1MA00479D.
37. Song, J.; Liu, H.; Zhao, Z.; Lin, P.; Yan, F. Flexible Organic Transistors for Biosensing: Devices and Applications. *Adv. Mater.* **2024**, *36*, 1–49, doi:10.1002/adma.202300034.
38. Lu, Z.; Xu, K.; Xiao, K.; Xu, Q.; Wang, L.; Li, P.; Zhou, J.; Zhao, D.; Bai, L.; Cheng, Y.; et al. Biomolecule sensors based on organic electrochemical transistors. *npj Flex. Electron.* **2025**, *9*, 9, doi:10.1038/s41528-025-00383-x.
39. Zhao, C.; Yang, J.; Ma, W. Transient Response and Ionic Dynamics in Organic Electrochemical Transistors. *Nano-Micro Lett.* **2024**, *16*, 233, doi:10.1007/s40820-024-01452-y.
40. Liao, C.; Mak, C.; Zhang, M.; Chan, H.L.W.; Yan, F. Flexible Organic Electrochemical Transistors for Highly Selective Enzyme Biosensors and Used for Saliva Testing. *Adv. Mater.* **2015**, *27*, 676–681, doi:10.1002/adma.201404378.
41. Fu, Y.; Wang, N.; Yang, A.; Law, H.K.; Li, L.; Yan, F. Highly Sensitive Detection of Protein Biomarkers with Organic Electrochemical Transistors. *Adv. Mater.* **2017**, *29*, doi:10.1002/adma.201703787.
42. Zhang, S.; Xia, C.; Wang, J.; Chen, S.; Wang, Y.; Zhang, S.; Geng, Z.; Tang, K.; Erdem, A.; Zhu, B. Ready-to-Use OECT Biosensor toward Rapid and Real-Time Protein Detection in Complex Biological Environments. *ACS Sensors* **2025**, *10*, 3369–3380, doi:10.1021/acssensors.4c03072.
43. Currano, L.J.; Sage, F.C.; Hagedon, M.; Hamilton, L.; Patrone, J.; Gerasopoulos, K. Wearable Sensor System for Detection of Lactate in Sweat. *Sci. Rep.* **2018**, *8*, 15890, doi:10.1038/s41598-018-33565-x.
44. Braendlein, M.; Pappa, A.; Ferro, M.; Lopresti, A.; Acquaviva, C.; Mamessier, E.; Malliaras, G.G.; Owens, R.M. Lactate Detection in Tumor Cell Cultures Using Organic Transistor Circuits. *Adv. Mater.* **2017**, *29*, 1–6, doi:10.1002/adma.201605744.
45. He, Y.; Kukhta, N.A.; Marks, A.; Luscombe, C.K. The effect of side chain engineering on conjugated polymers in organic electrochemical transistors for bioelectronic applications. *J. Mater. Chem. C* **2022**, *10*, 2314–2332, doi:10.1039/D1TC05229B.
46. Montero-Jimenez, M.; Lugli-Arroyo, J.; Fenoy, G.E.; Piccinini, E.; Knoll, W.; Marmisollé, W.A.; Azzaroni, O. Transduction of Amine–Phosphate Supramolecular Interactions and Biosensing of Acetylcholine through PEDOT-Polyamine Organic Electrochemical Transistors. *ACS Appl. Mater. Interfaces* **2023**, doi:10.1021/acsami.3c09286.
47. Fenoy, G.E.; Scotto, J.; Allegretto, J.A.; Piccinini, E.; Cantillo, A.L.; Knoll, W.; Azzaroni, O.; Marmisollé, W.A. Layer-by-Layer Assembly Monitored by PEDOT-Polyamine-Based Organic Electrochemical Transistors. *ACS Appl. Electron. Mater.* **2022**, *4*, 5953–5962, doi:10.1021/acsaelm.2c01124.
48. Fenoy, G.E.; Hasler, R.; Lorenz, C.; Movilli, J.; Marmisollé, W.A.; Azzaroni, O.; Huskens, J.; Bäuerle, P.; Knoll, W. Interface Engineering of "Clickable" Organic Electrochemical Transistors toward Biosensing Devices. *ACS Appl. Mater. Interfaces* **2023**, *15*, 10885–10896, doi:10.1021/acsami.2c21493.
49. Liu, H.; Song, J.; Zhao, Z.; Zhao, S.; Tian, Z.; Yan, F. Organic Electrochemical Transistors for Biomarker Detections. *Adv. Sci.* **2024**, *11*, doi:10.1002/advs.202305347.
50. Khodagholy, D.; Rivnay, J.; Sessolo, M.; Gurfinkel, M.; Leleux, P.; Jimison, L.H.; Stavrinidou, E.; Herve, T.; Sanaur, S.; Owens, R.M.; et al. High transconductance organic electrochemical transistors. *Nat. Commun.* **2013**, *4*, 1–6, doi:10.1038/ncomms3133.
51. Wang, L.; Yue, X.; Sun, Q.; Zhang, L.; Ren, G.; Lu, G.; Yu, H.-D.; Huang, W. Flexible organic electrochemical transistors for chemical and biological sensing. *Nano Res.* **2022**, *15*, 2433–2464, doi:10.1007/s12274-021-3856-3.
52. Piro, B.; Mattana, G.; Zrig, S.; Anquetin, G.; Battaglini, N.; Capitao, D.; Maurin, A.; Reisberg, S. Fabrication and Use of Organic Electrochemical Transistors for Sensing of Metabolites in Aqueous Media. *Appl. Sci.* **2018**, *8*, 928, doi:10.3390/app8060928.

 doi:10.20944/preprints202512.0526.v1

53. Wang, Y.; Zhou, Z.; Qing, X.; Zhong, W.; Liu, Q.; Wang, W.; Li, M.; Liu, K.; Wang, D. Ion sensors based on novel fiber organic electrochemical transistors for lead ion detection. *Anal. Bioanal. Chem.* **2016**, *408*, 5779–5787, doi:10.1007/s00216-016-9684-8.
54. Tan, S.T.M.; Keene, S.; Giovannitti, A.; Melianas, A.; Moser, M.; McCulloch, I.; Salleo, A. Operation mechanism of organic electrochemical transistors as redox chemical transducers. *J. Mater. Chem. C* **2021**, *9*, 12148–12158, doi:10.1039/D1TC02224E.
55. Schafer, E.A.; Wu, R.; Meli, D.; Tropp, J.; Moser, M.; McCulloch, I.; Paulsen, B.D.; Rivnay, J. Sources and Mechanism of Degradation in p-Type Thiophene-Based Organic Electrochemical Transistors. *ACS Appl. Electron. Mater.* **2022**, *4*, 1391–1404, doi:10.1021/acsaelm.1c01171.
56. Zhang, S.; Ding, P.; Ruoko, T.; Wu, R.; Stoeckel, M.; Massetti, M.; Liu, T.; Vagin, M.; Meli, D.; Kroon, R.; et al. Toward Stable p-Type Thiophene-Based Organic Electrochemical Transistors. *Adv. Funct. Mater.* **2023**, *33*, doi:10.1002/adfm.202302249.
57. Hu, Z.; Hu, Y.; Huang, L.; Zhong, W.; Zhang, J.; Lei, D.; Chen, Y.; Ni, Y.; Liu, Y. Recent Progress in Organic Electrochemical Transistor-Structured Biosensors. *Biosensors* **2024**, *14*, 330, doi:10.3390/bios14070330.
58. Keene, S.T.; Fogarty, D.; Cooke, R.; Casadevall, C.D.; Salleo, A.; Parlak, O. Wearable Organic Electrochemical Transistor Patch for Multiplexed Sensing of Calcium and Ammonium Ions from Human Perspiration. *Adv. Healthc. Mater.* **2019**, *8*, 1–8, doi:10.1002/adhm.201901321.
59. Gualandi, I.; Marzocchi, M.; Scavetta, E.; Calienni, M.; Bonfiglio, a.; Fraboni, B. A simple all-PEDOT:PSS electrochemical transistor for ascorbic acid sensing. *J. Mater. Chem. B* **2015**, *3*, 6753–6762, doi:10.1039/C5TB00916B.
60. Wang, Y.; Qing, X.; Zhou, Q.; Zhang, Y.; Liu, Q.; Liu, K.; Wang, W.; Li, M.; Lu, Z.; Chen, Y.; et al. The woven fiber organic electrochemical transistors based on polypyrrole nanowires/reduced graphene oxide composites for glucose sensing. *Biosens. Bioelectron.* **2017**, *95*, 138–145, doi:10.1016/j.bios.2017.04.018.
61. Ji, W.; Wu, D.; Tang, W.; Xi, X.; Su, Y.; Guo, X.; Liu, R. Carbonized silk fabric-based flexible organic electrochemical transistors for highly sensitive and selective dopamine detection. *Sensors Actuators B Chem.* **2020**, *304*, 127414, doi:10.1016/j.snb.2019.127414.
62. Majak, D.; Fan, J.; Kang, S.; Gupta, M. Delta-9-tetrahydrocannabinol (Δ 9 -THC) sensing using an aerosol jet printed organic electrochemical transistor (OECT). *J. Mater. Chem. B* **2021**, *9*, 2107–2117, doi:10.1039/D0TB02951C.
63. Wang, Y.; Xiong, C.; Qu, H.; Chen, W.; Ma, A.; Zheng, L. Highly sensitive real-time detection of tyrosine based on organic electrochemical transistors with poly-(diallyldimethylammonium chloride), gold nanoparticles and multi-walled carbon nanotubes. *J. Electroanal. Chem.* **2017**, *799*, 321–326, doi:10.1016/j.jelechem.2017.06.033.
64. Tang, H.; Yan, F.; Lin, P.; Xu, J.; Chan, H.L.W. Highly Sensitive Glucose Biosensors Based on Organic Electrochemical Transistors Using Platinum Gate Electrodes Modified with Enzyme and Nanomaterials. *Adv. Funct. Mater.* **2011**, *21*, 2264–2272, doi:10.1002/adfm.201002117.
65. Fenoy, G.E.; von Bilderling, C.; Knoll, W.; Azzaroni, O.; Marmisollé, W.A. PEDOT:Tosylate-Polyamine-Based Organic Electrochemical Transistors for High-Performance Bioelectronics. *Adv. Electron. Mater.* **2021**, *7*, 2100059, doi:10.1002/aelm.202100059.
66. Montero-Jimenez, M.; Neyra Recky, J.R.; von Bilderling, C.; Scotto, J.; Azzaroni, O.; Marmisollé, W.A. PEDOT: Tosylate-polyamine-based enzymatic organic electrochemical transistors for high-performance glucose biosensing in human urine samples. *J. Electroanal. Chem.* **2025**, *978*, 118867, doi:10.1016/j.jelechem.2024.118867.
67. Neyra Recky, J.R.; Montero-Jimenez, M.; Scotto, J.; Azzaroni, O.; Marmisollé, W.A. Urea Biosensing through Integration of Urease to the PEDOT-Polyamine Conducting Channels of Organic Electrochemical Transistors: pH-Change-Based Mechanism and Urine Sensing. *Chemosensors* **2024**, *12*, 124, doi:10.3390/chemosensors12070124.
68. Sappia, L.D.; Piccinini, E.; von Binderling, C.; Knoll, W.; Marmisollé, W.; Azzaroni, O. PEDOT-polyamine composite films for bioelectrochemical platforms - flexible and easy to derivatize. *Mater. Sci. Eng. C* **2020**, *109*, 110575, doi:10.1016/j.msec.2019.110575.

69. Wang, Y.; Wustoni, S.; Surgailis, J.; Zhong, Y.; Koklu, A.; Inal, S. Designing organic mixed conductors for electrochemical transistor applications. *Nat. Rev. Mater.* **2024**, *9*, 249–265, doi:10.1038/s41578-024-00652-7.
70. Yu, S.; Ratcliff, E.L. Tuning Organic Electrochemical Transistor (OECT) Transconductance toward Zero Gate Voltage in the Faradaic Mode. *ACS Appl. Mater. Interfaces* **2021**, *13*, 50176–50186, doi:10.1021/acsami.1c13009.
71. Montero-Jimenez, M.; Amante, F.L.; Fenoy, G.E.; Scotto, J.; Azzaroni, O.; Marmisolle, W.A. PEDOT-Polyamine-Based Organic Electrochemical Transistors for Monitoring Protein Binding. *Biosensors* **2023**, *13*, 288, doi:10.3390/bios13020288.
72. Ravariu, C. From Enzymatic Dopamine Biosensors to OECT Biosensors of Dopamine. *Biosensors* **2023**, *13*, 806, doi:10.3390/bios13080806.
73. Gualandi, I.; Tessarolo, M.; Mariani, F.; Arcangeli, D.; Possanzini, L.; Tonelli, D.; Fraboni, B.; Scavetta, E. Layered Double Hydroxide-Modified Organic Electrochemical Transistor for Glucose and Lactate Biosensing. *Sensors* **2020**, *20*, 3453, doi:10.3390/s20123453.
74. Tang, K.; Turner, C.; Case, L.; Mehrehjedy, A.; He, X.; Miao, W.; Guo, S. Organic Electrochemical Transistor with Molecularly Imprinted Polymer-Modified Gate for the Real-Time Selective Detection of Dopamine. *ACS Appl. Polym. Mater.* **2022**, *4*, 2337–2345, doi:10.1021/acsapm.1c01563.
75. Fenoy, G.E.; Azzaroni, O.; Knoll, W.; Marmisollé, W.A. Functionalization Strategies of PEDOT and PEDOT:PSS Films for Organic Bioelectronics Applications. *Chemosensors* **2021**, *9*, 212, doi:10.3390/chemosensors9080212.
76. Shoaie, N.; Daneshpour, M.; Azimzadeh, M.; Mahshid, S.; Khoshfetrat, S.M.; Jahanpeyma, F.; Gholaminejad, A.; Omidfar, K.; Foruzandeh, M. Electrochemical sensors and biosensors based on the use of polyaniline and its nanocomposites: a review on recent advances. *Microchim. Acta* **2019**, *186*, 465, doi:10.1007/s00604-019-3588-1.
77. Demuru, S.; Kunnel, B.P.; Briand, D. Thin film organic electrochemical transistors based on hybrid PANI/PEDOT:PSS active layers for enhanced pH sensing. *Biosens. Bioelectron. X* **2021**, *7*, 100065, doi:10.1016/j.biosx.2021.100065.
78. Wang, Z.; Liu, M.; Zhao, Y.; Chen, Y.; Noureen, B.; Du, L.; Wu, C. Functional Organic Electrochemical Transistor-Based Biosensors for Biomedical Applications. *Chemosensors* **2024**, *12*, 236, doi:10.3390/chemosensors12110236.
79. Gao, N.; Yu, J.; Tian, Q.; Shi, J.; Zhang, M.; Chen, S.; Zang, L. Application of pedot:Pss and its composites in electrochemical and electronic chemosensors. *Chemosensors* **2021**, *9*, doi:10.3390/chemosensors9040079.
80. Kawamura, R.; Michinobu, T. PEDOT:PSS versus Polyaniline: A Comparative Study of Conducting Polymers for Organic Electrochemical Transistors. *Polymers (Basel).* **2023**, *15*, 4657, doi:10.3390/polym15244657.
81. Paasch, G.; Scheinert, S.; Herasimovich, A.; Hörselmann, I.; Lindner, T. Characteristics and mechanisms of hysteresis in polymer field-effect transistors. *Phys. status solidi* **2008**, *205*, 534–548, doi:10.1002/pssa.200723400.
82. Scotto, J.; Florit, M.I.; Posadas, D. pH dependence of the voltammetric response of Polyaniline. *J. Electroanal. Chem.* **2017**, *785*, 14–19, doi:10.1016/j.jelechem.2016.11.066.